Electronic Supplementary Material (ESI) for New Journal of Chemistry.

Electrocatalytic proton reduction by dinuclear cobalt complexes in a nonaqueous electrolyte

Manaswini Raj [a] and Sumanta Kumar Padhi [a], *

[a]*Artificial Photosynthesis Laboratory, Department of Chemistry and Chemical Biology, Indian Institute of Technology (Indian School of Mines), Dhanbad, 826004.*
Email: sumanta@iitism.ac.in

Supporting Information

Experimental Section

Materials and methods

Materials: All the reagent-grade commercially accessible chemicals employed in this work were procured from Alfa Aesar and Sigma Aldrich and were utilized as received without any further purification. All the analytical-grade organic solvents used were purchased from Merck, purified from solvent purification system followed by drying of solvents before use. HPLC grade solvents were purchased from Merck and used for electrochemical as well as optical studies.

Optical Measurements. UV-Vis spectra performed in this work were recorded on Agilent Technologies Cary 8454 photodiode array UV–Visible spectrophotometer.

Mass spectroscopy. High-resolution ESI mass spectra were performed by an Agilent Technologies 1290 Infinity UHPLC System and Bruker micrOTOF-Q II instruments.

X-ray crystallography. X-ray diffraction data for all the suitable single crystals of the complexes were collected using a Rigaku SuperNova G8910B EosS2 single-crystal X-ray diffractometer with Mo Kα radiation (λ = 0.71073 Å) which is equipped with an EosS2 CCD detector for the assemblage of frames. The data integration and establishment of the unit cell were carried out by CrysAlis^{Pro} software.[1] The data collection was done at 293 K and structures were solved by using Olex2 software through the Charge Flipping solution program.[2] The Olex2 refinement package was operated for the structural data refinement by using Gauss-Newton minimization.[3] In case complex **2**, the hydrogen atoms for 1.75 water molecules neither be detected nor identified.

Electrochemistry. The electrochemical analysis was performed using ALS/CHI model 1140C electrochemical analyzer. All electrochemical measurements were carried out in a three-electrode configuration filled with 0.1 M tetrabutylammonium perchlorate ($^{n}Bu_4NClO_4$, TBAP) used as supporting electrolyte in 95/5 (v/v) DMF/H_2O solution under inert atmosphere. In this work, glassy carbon electrode (A= 0.07 cm^2), platinum wire, and saturated calomel electrode were used as working, counter, and reference electrodes respectively. Before every scan, the glassy carbon electrode was polished and cleaned using alumina oxide paste. The electrocatalytic studies of the complexes for reduction event were examined in three different concentrations; 0.50 mM, 0.75 mM, and 1.0 mM using CH_3COOH as the proton source. The Electrochemical Impedance spectroscopy(EIS) analysis was performed on the CH instrument model 660D electrochemical analyzer. The experiment was conducted in 95/5 (v/v) DMF/H_2O solution at -1.5 V vs SCE with the addition of 24 equivalent of acetic acid as the proton source.

Controlled potential coulometry. A custom-made air-tight electrolytic cell was used to perform the controlled potential experiments for all the complexes. Glassy carbon rod, platinum mesh, and saturated calomel electrode were used as working, auxiliary, and reference electrodes respectively. 0.5 mM from each complex were examined in 95/5 (v/v) DMF/H_2O solution containing 0.1 M $^{n}Bu_4NClO_4$ as supporting electrolyte with the addition of 24 equivalent of CH_3COOH as the proton source. Experiments were carried out for half an hour under inert conditions at room temperature.

Hydrogen evolution studies. GC analysis of evolved gas was performed at the end of the controlled potential experiment using Michro-9100 Gas chromatograph (Netel India limited) equipped with TCD detector using He as the carrier gas. The gas sample collected at the headspace aliquots was collected by using Hamilton gas-tight syringe which upon injection was detected and analyzed by the instrument.

Spectro-electrochemistry. The UV-Vis spectroelectrochemical studies were performed using CHI 1140 and 8454 UV-Vis spectrophotometer for monitoring the electrochemical and spectral changes respectively. The experiment was carried out using a three-electrode configuration in a Quartz cuvette containing 3 mL of 0.05 mM catalysts with the addition of 24 equivalent of CH_3COOH as the proton source under an inert atmosphere for a duration of half an hour. The Pt mesh, Pt wire, and Ag wire were used as working, counter, and reference electrodes respectively.

FESEM and EDX studies. The surface morphology of the glassy carbon plate was studied by Supra 55 (Carl Zeiss, Germany) field-emission scanning electron microscopy (FESEM) system.

Synthesis of $[Co^{II}_2(L^1)_2]$ (1). The one equivalent of ligand, **L^1** (2-{[2-(8-hydroxyquinolin-2-yl)-1*H*-benzimidazol-1-yl]methyl}quinolin-8-ol), (0.1 g, 0.23 mmol) was dissolved in the minimum amount of DCM and CH_3OH solvent mixture, to which one equivalent of $Co(CH_3COO)_2.4H_2O$ (0.059 g, 0.23 mmol) dissolved in methanolic solution was added dropwise into it and was stirred for 4-5 h at room temperature. The volume of the reaction solution was reduced under vacuum resulting in a yellowish precipitate which was washed with ice-cold CH_3OH followed by excess diethyl ether and finally dried in vacuo. The slow evaporation of the resulting product in DMF medium results in brown-colored crystals. Yield (52 % concerning Co metal center). Calculated mass for $[C_{52}H_{32}Co_2N_8O_4]$ = 950.12; found value= 950.79. Anal. Calcd for $[Co(L^1)]_2 \cdot H_2O$, $C_{52}H_{34}Co_2N_8O_5$: C, 64.47; H, 3.54; N, 11.57. Found: C, 64.51; H, 3.58; N, 11.63.

Synthesis of $[Co^{II}_2(L^2)_2]$ (2). To the solution of one equivalent of ligand, **L^2** (2-{[6-methyl-2-(8-hydroxyquinolin-2-yl)-1*H*-benzimidazol-1-yl]methyl}quinolin-8-ol)), (0.1 g, 0.23 mmol) in DCM and CH_3OH mixture, one equivalent of methanolic solution of $Co(CH_3COO)_2.4H_2O$ (0.057 g, 0.23 mmol) was added dropwise. The reaction mixture was then stirred for 4-5 h at room temperature. It was then reduced to the minimum volume under vacuum. The obtained yellow precipitate was washed several times with ice-cold CH_3OH and then with diethyl ether. The resulting precipitate was dried in vacuo. It was dissolved in DMF solvent that yielded suitable brown colored single crystals for crystallographic analysis. Yield (47 % concerning Co metal center). Calculated mass for $[C_{54}H_{36}Co_2N_8O_4 + H^+]$ = 979.15; found value= 979.16. Anal. Calcd for $[Co(L^2)]_2 \cdot 6.75H_2O$, $C_{54}H_{49.5}Co_2N_8O_{10.5}$: C, 58.94; H, 4.53; N, 10.18. Found: C, 60.11; H, 4.58; N, 10.32.

Table S1. Crystal data and structure refinement for $[Co(L^1)]_2.H_2O$

CCDC code	2096756
Empirical formula	$C_{26}H_{18}CoN_4O_3$
Formula weight	493.39
Temperature/K	293
Crystal system	trigonal
Space group	$P3_121$
a/Å	13.3668(6)
b/Å	13.3668(6)
c/Å	20.7353(10)
α/°	90
β/°	90
γ/°	120
Volume/Å^3	3208.5(3)
Z	6
ρ_{calc}g/cm^3	1.5320
μ/mm^{-1}	0.841
F(000)	1520.7
Crystal size/mm^3	0.24 × 0.22 × 0.2
Radiation	Mo Kα (λ = 0.71073)
2Θ range for data collection/°	6.86 to 58.3
Index ranges	-11 ≤ h ≤ 16, -5 ≤ k ≤ 17, -28 ≤ l ≤ 26
Reflections collected	7912
Independent reflections	4371 [R_{int} = 0.0213, R_{sigma} = 0.0424]
Data/restraints/parameters	4371/0/312
Goodness-of-fit on F^2	1.048

Final R indexes [I>=2σ (I)]	R_1 = 0.0420, wR_2 = 0.0965
Final R indexes [all data]	R_1 = 0.0547, wR_2 = 0.1029
Largest diff. peak/hole / e Å^{-3}	0.41/-0.29

Table S2. Crystal data and structure refinement for $[Co(L^2)]_2.6.75H_2O$

Identification code	2096757
Empirical formula	$C_{54}H_{49.5}Co_2N_8O_{10.5}$
Formula weight	1054.77
Temperature/K	293(2)
Crystal system	monoclinic
Space group	$P2_1/n$
a/Å	12.9630(8)
b/Å	15.6404(8)
c/Å	25.9135(14)
α/°	90
β/°	101.410(5)
γ/°	90
Volume/Å^3	5150.0(5)
Z	4
ρ_{calc}g/cm^3	1.415
μ/mm^{-1}	0.713
F(000)	2156.0
Crystal size/mm^3	0.26 × 0.24 × 0.19
Radiation	MoKα (λ = 0.71073)
2Θ range for data collection/°	4.132 to 49.488
Index ranges	-10 ≤ h ≤ 15, -18 ≤ k ≤ 17, -30 ≤ l ≤ 30
Reflections collected	19993
Independent reflections	8459 [R_{int} = 0.0386, R_{sigma} = 0.0545]
Data/restraints/parameters	8459/0/693
Goodness-of-fit on F^2	1.023
Final R indexes [I>=2σ (I)]	R_1 = 0.0630, wR_2 = 0.1548
Final R indexes [all data]	R_1 = 0.0914, wR_2 = 0.1792
Largest diff. peak/hole / e Å^{-3}	0.90/-0.38

Table S3. Bond Lengths for 1.

Atom	Atom	Length/Å
Co1	O2	1.968(2)
Co1	N3	2.114(3)
Co1	O1	2.024(2)
Co1	N1	2.120(3)
Co1	N4	2.208(3)

Table S4. Bond Angles for 1.			
Atom	**Atom**	**Atom**	**Angle/°**
N3	Co1	O2	131.04(10)
O1[1]	Co1	O2	88.25(11)
O1[1]	Co1	N3	96.15(10)
N1[1]	Co1	O2	123.69(10)
N1[1]	Co1	N3	105.10(10)
N1[1]	Co1	O1[1]	81.10(10)
N4[1]	Co1	O2	79.01(10)
N4[1]	Co1	N3	93.54(10)
N4[1]	Co1	O1[1]	167.14(11)
N4[1]	Co1	N1[1]	104.51(10)

Table S5. Bond Lengths for 2.		
Atom	**Atom**	**Length/Å**
Co1	O2	1.958(3)
Co1	O1	2.033(3)
Co1	N1	2.127(3)
Co1	N4	2.228(3)
Co1	N7	2.087(4)
Co2	O4	1.973(3)
Co2	N8	2.194(3)
Co2	N3	2.065(3)
Co2	O3	2.009(3)
Co2	N5	2.142(4)

Table S6. Bond Angles for 2.			
Atom	**Atom**	**Atom**	**Angle/°**
O2	Co1	O1	91.30(13)
O2	Co1	N1	119.86(12)
O2	Co1	N4	77.76(12)
O2	Co1	N7	126.28(13)
O1	Co1	N1	80.13(12)
O1	Co1	N4	168.34(13)
O1	Co1	N7	94.98(13)
N1	Co1	N4	101.67(11)
N7	Co1	N1	113.78(12)
N7	Co1	N4	94.78(11)
O4	Co2	N8	78.26(13)
O4	Co2	N3	122.15(12)
O4	Co2	O3	92.98(15)
O4	Co2	N5	121.59(13)
N3	Co2	N8	93.39(11)
N3	Co2	N5	116.24(14)
O3	Co2	N8	169.86(14)
O3	Co2	N3	95.63(14)
O3	Co2	N5	79.93(14)
N5	Co2	N8	100.19(13)

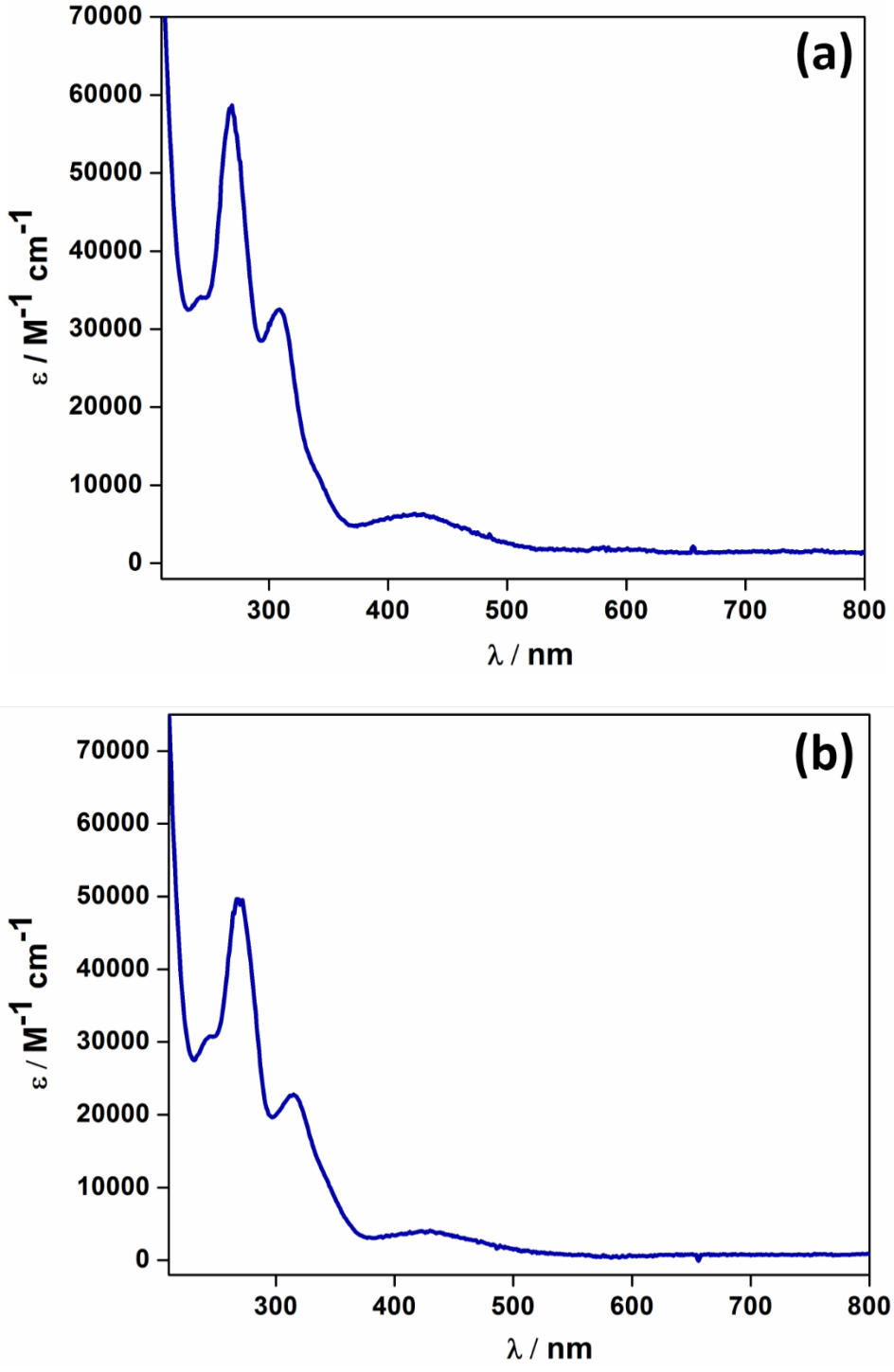

Figure S1. The UV-Vis spectra of (a) **1** ($0.01x10^{-3}$ M) and (b) **2** ($0.01x10^{-3}$ M) in methanol.

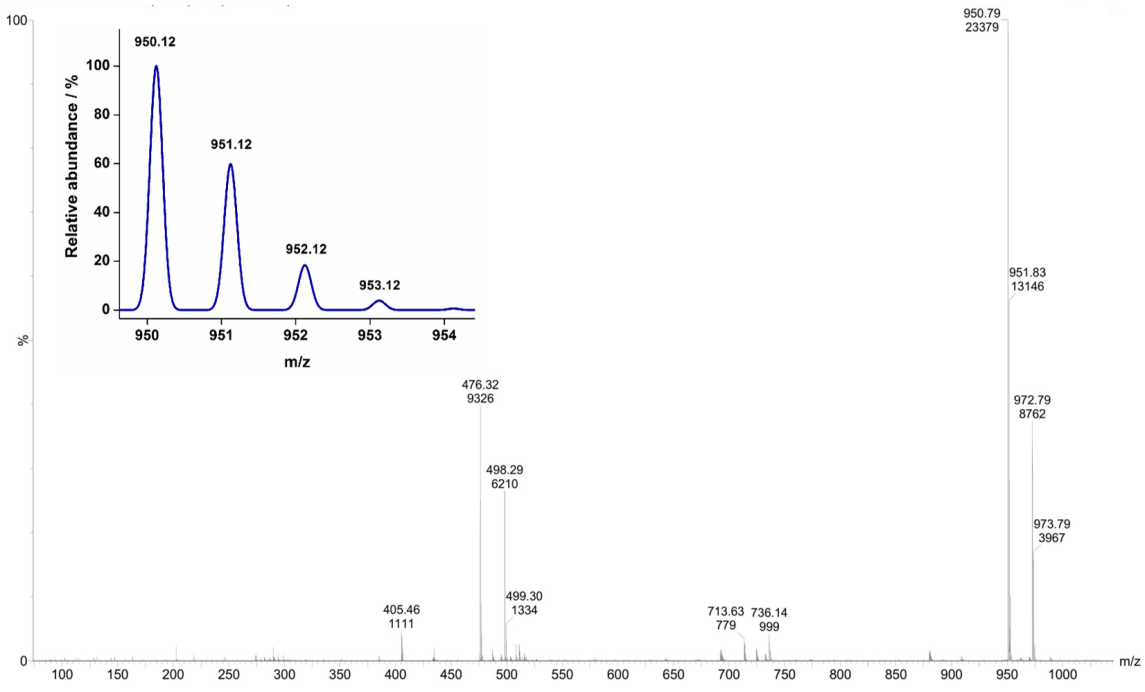

Figure S2. Mass spectra of **1** in DMF.

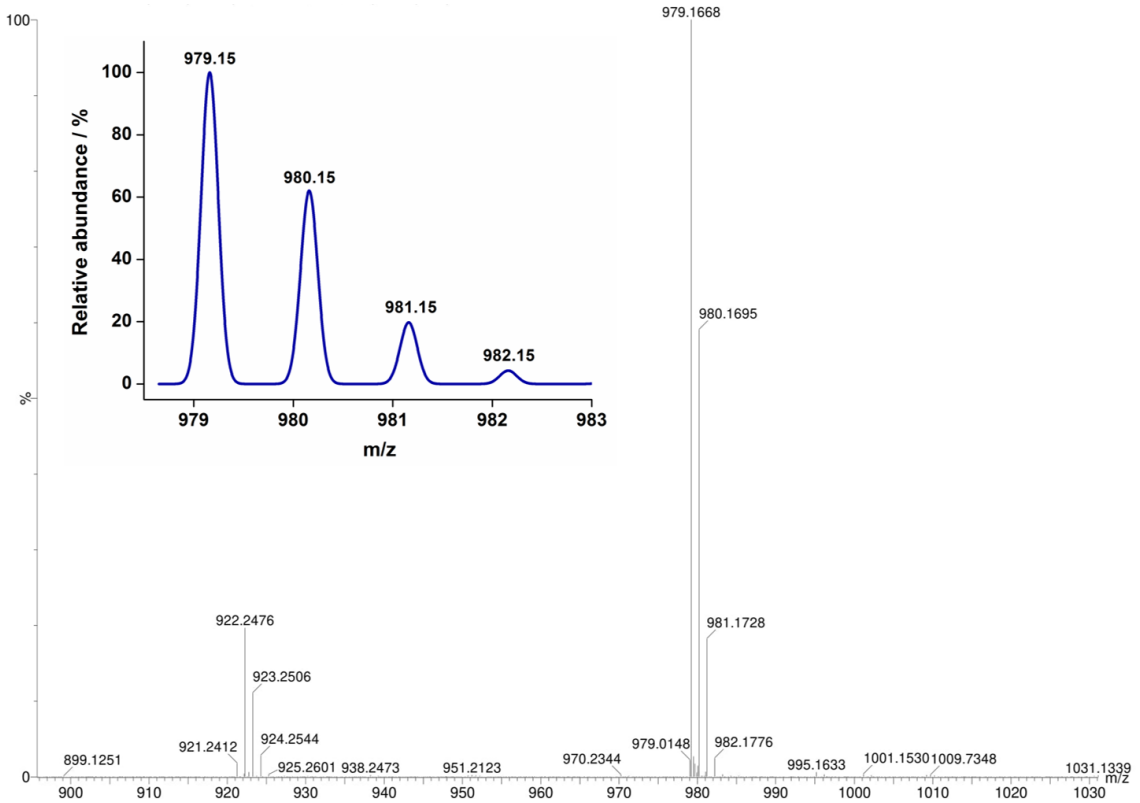

Figure S3. Mass spectra of **2** in DMF.

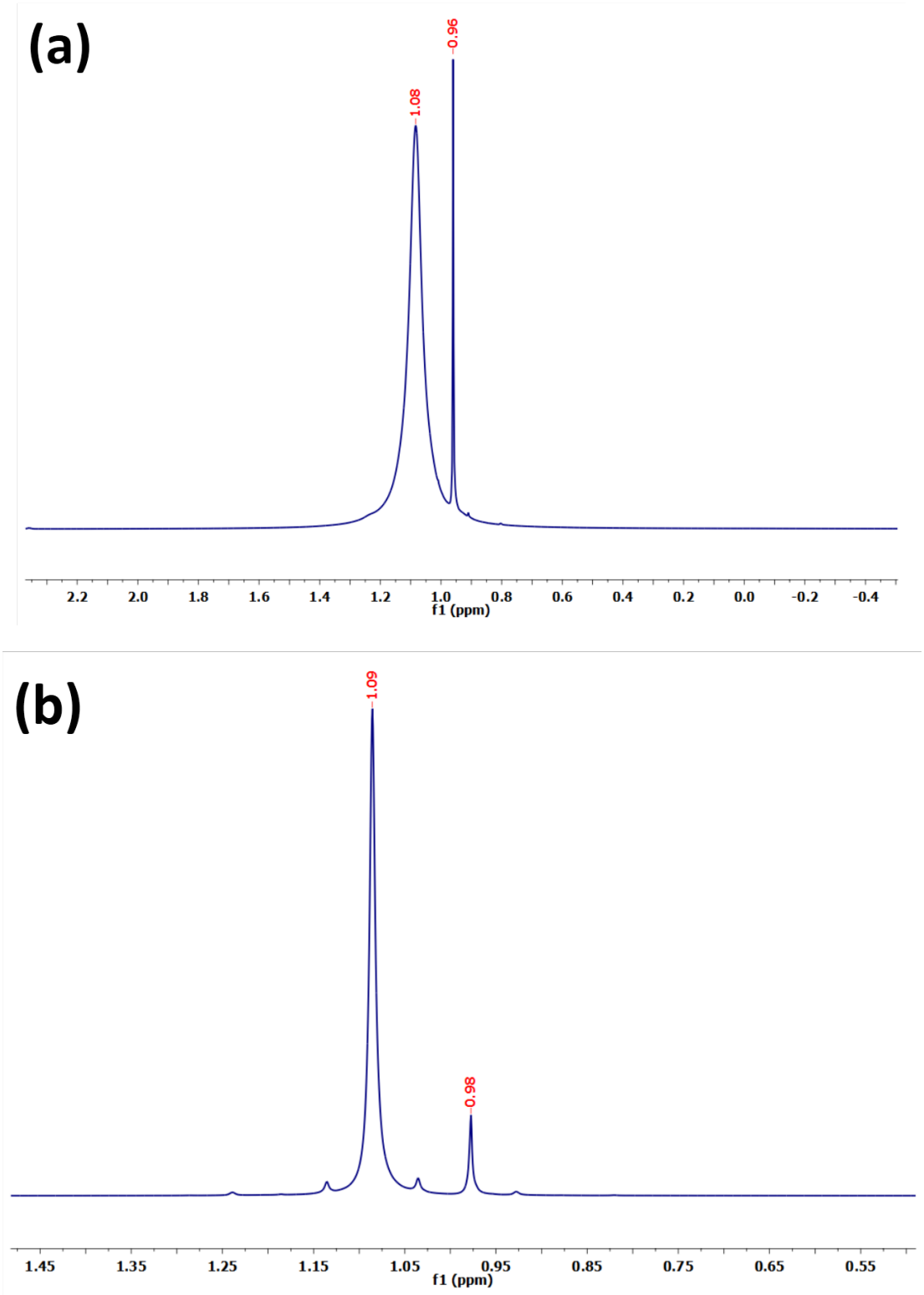

Figure S4. ^{1}H NMR spectra of *t*-BuOH for measurement of magnetic susceptibility of (a) **1** and (b) **2** by Evans method in 10 % *t*-BuOH and DMSO mixture at 25°C.

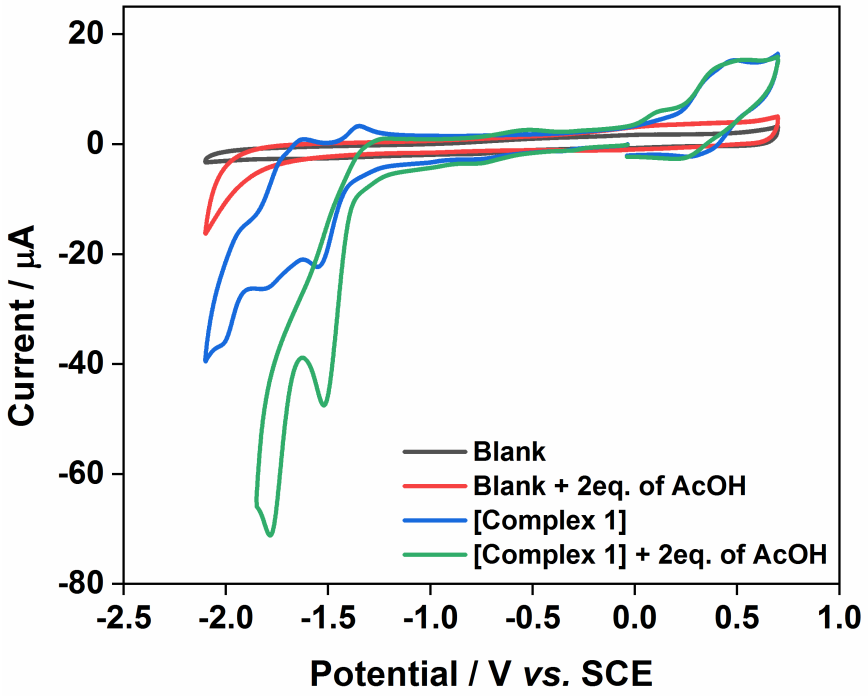

Figure S5. Cyclic voltammogram of blank (grey) and **1** (blue) and after addition of 2 equivalent of AcOH to blank (red) and **1** (green). Electrocatalytic condition: 1.0 mM of the complex in 95/5 (v/v) DMF/H_2O with 0.1 M TBAP as supporting electrolyte at a scan rate of 100 mV s^{-1} under an inert atmosphere using a three-electrode configuration.

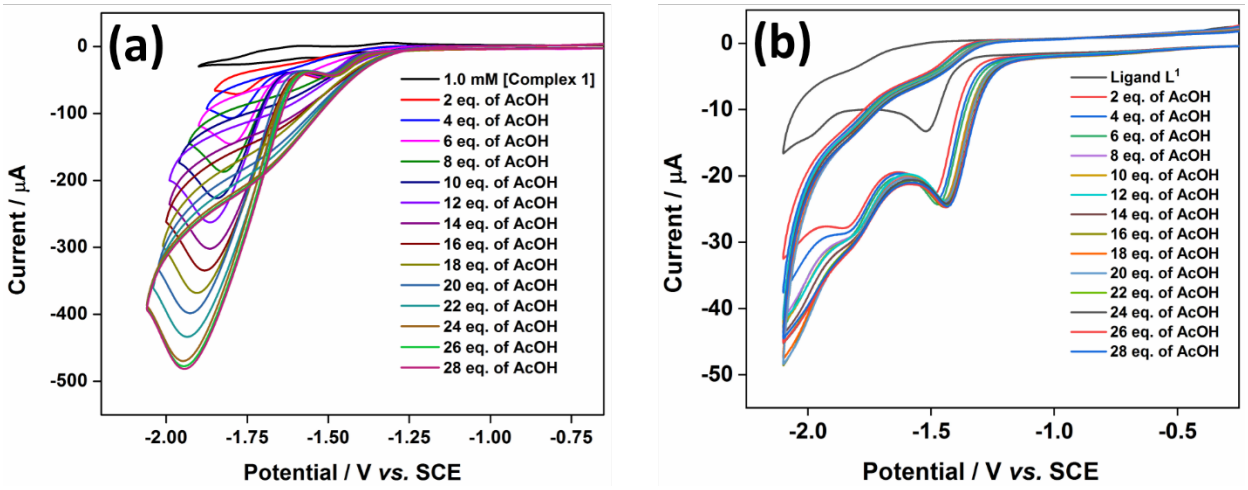

Figure S6. Electrocatalytic proton reduction by 1.0 mM of (a) **1** and ligand (b) **L^1**. Electrocatalytic condition: **1** and **L^1** and in 95/5 (v/v) DMF/H_2O in presence of 0.1 M TBAP as supporting electrolyte at a scan rate of 100 mV s^{-1} under an inert atmosphere using three-electrode configuration.

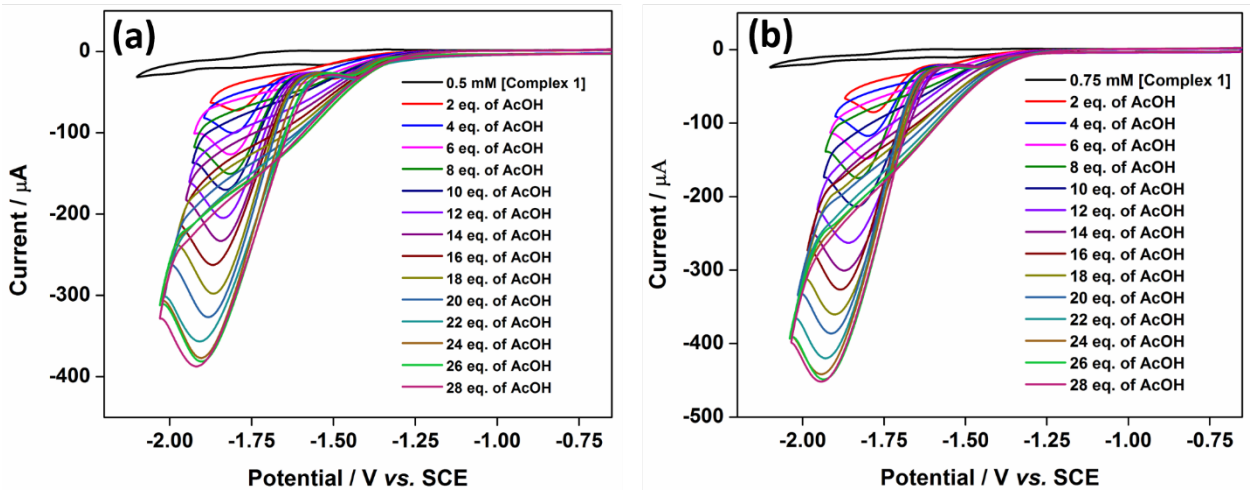

Figure S7. Electrocatalytic proton reduction by (a) 0.5 mM and (b) 0.75 mM of **1**. Electrocatalytic condition: **1** in 95/5 (v/v) DMF/H_2O in presence of 0.1 M TBAP as supporting electrolyte at a scan rate of 100 mV s^{-1} under inert atmosphere using three-electrode configuration.

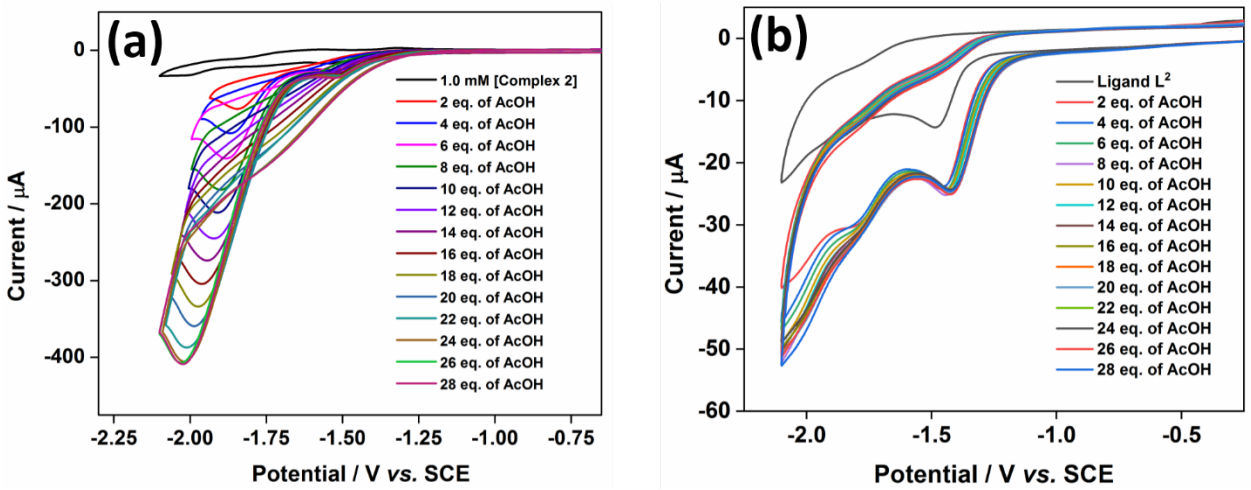

Figure S8. Electrocatalytic proton reduction by 1.0 mM of (a) **2** and ligand (b) **L²**. Electrocatalytic condition: **2** and **L²** and in 95/5 (v/v) DMF/H_2O in presence of 0.1 M TBAP as supporting electrolyte at a scan rate of 100 mV s^{-1} under an inert atmosphere using three-electrode configuration.

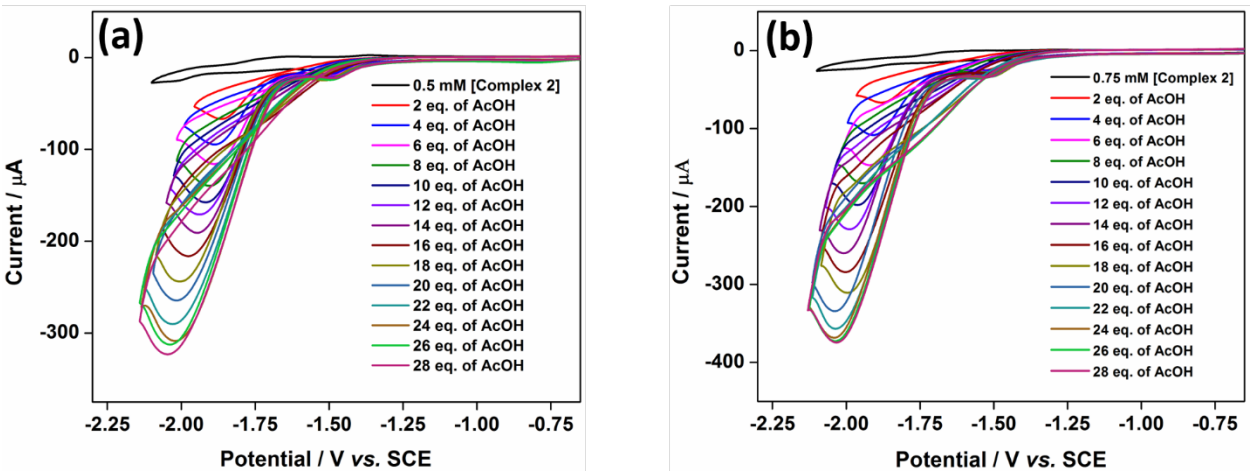

Figure S9. Electrocatalytic proton reduction by (a) 0.5 mM and (b) 0.75 mM of **2**. Electrocatalytic condition: **2** in 95/5 (v/v) DMF/H_2O in presence of 0.1 M TBAP as supporting electrolyte at a scan rate of 100 mV s^{-1} under inert atmosphere using three-electrode configuration.

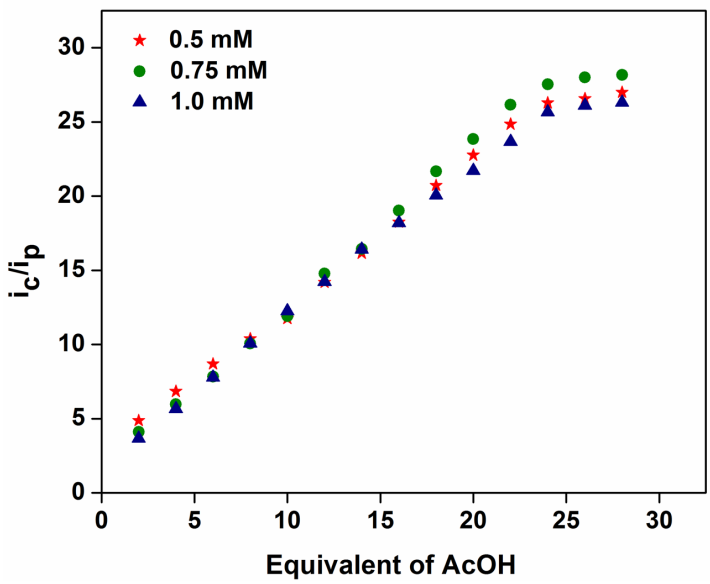

Figure S10. Plot of i_c/i_p *vs.* equivalents of AcOH for three distinct concentrations (0.5 mM, 0.75 mM and 1.0 mM) of **1**. Electrocatalytic condition: **1** in 95/5 (v/v) DMF/H_2O in presence of 0.1 M TBAP as supporting electrolyte at a scan rate of 100 mV s^{-1} under an inert atmosphere using three-electrode configuration.

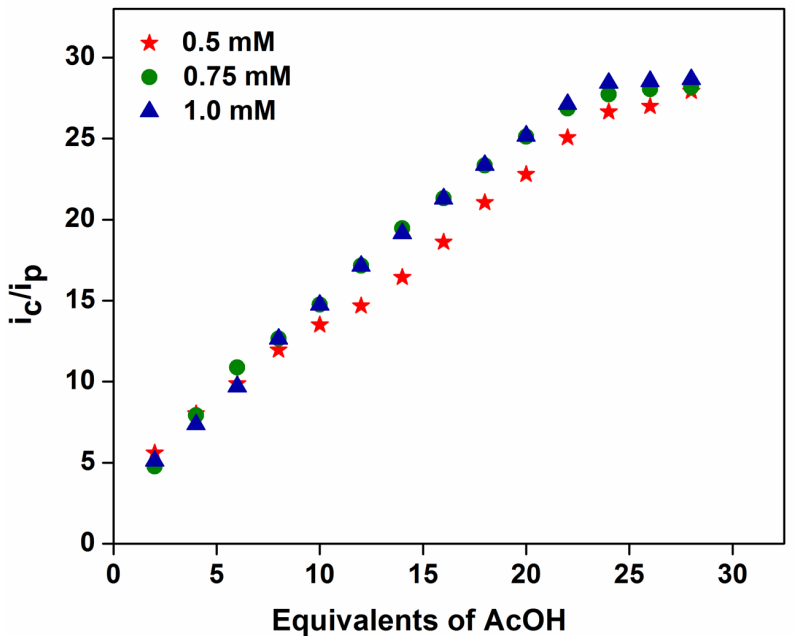

Figure S11. Plot of i_c/i_p *vs.* equivalents of AcOH for three distinct concentrations (0.5 mM, 0.75 mM and 1.0 mM) of **2**. Electrocatalytic condition: **2** in 95/5 (v/v) DMF/H_2O in presence of 0.1 M TBAP as supporting electrolyte at a scan rate of 100 mV s^{-1} under an inert atmosphere using three-electrode configuration.

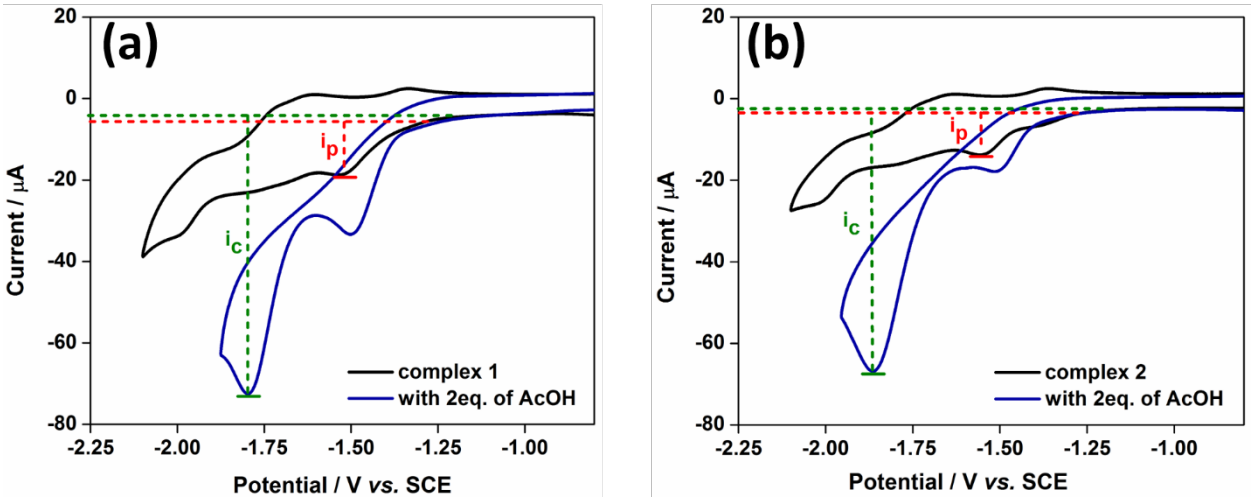

Figure S12. Plot displaying i_c and i_p current for **1** and **2**. Electrocatalytic condition: 0.5 mM of each complex **1** and **2** in 95/5 (v/v) DMF/H_2O in presence of 0.1 M TBAP as supporting electrolyte at a scan rate of 100 mV s^{-1} under an inert atmosphere using three-electrode configuration.

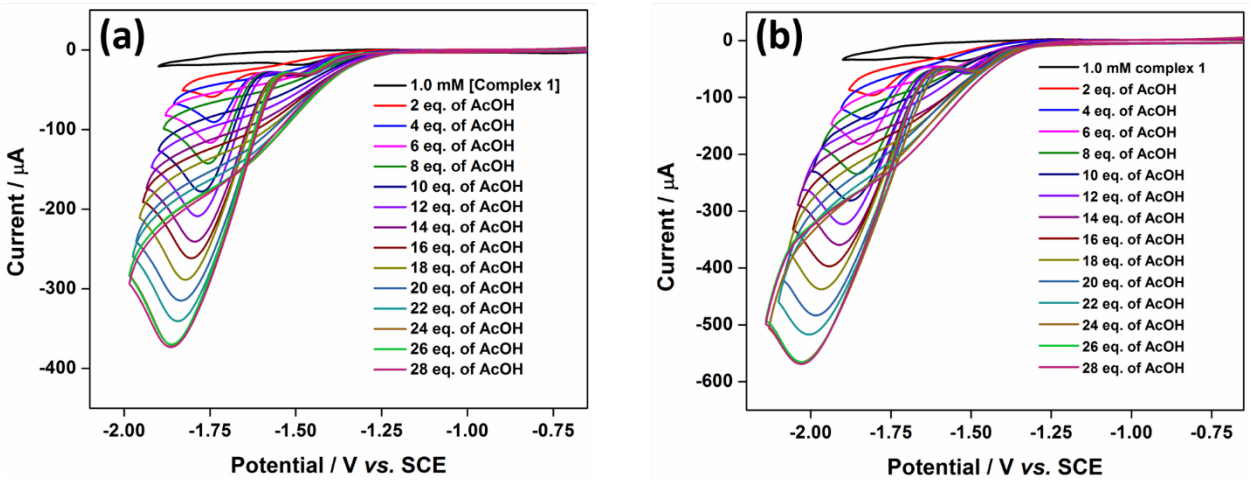

Figure S13. Electrocatalytic proton reduction by **1** at a scan rate of (a) 50 mV s^{-1} and (b) 150 mV s^{-1}. Electrocatalytic condition: 1.0 mM of **1** in 95/5 (v/v) DMF/H_2O in presence of 0.1 M TBAP as supporting electrolyte under inert atmosphere using three-electrode configuration.

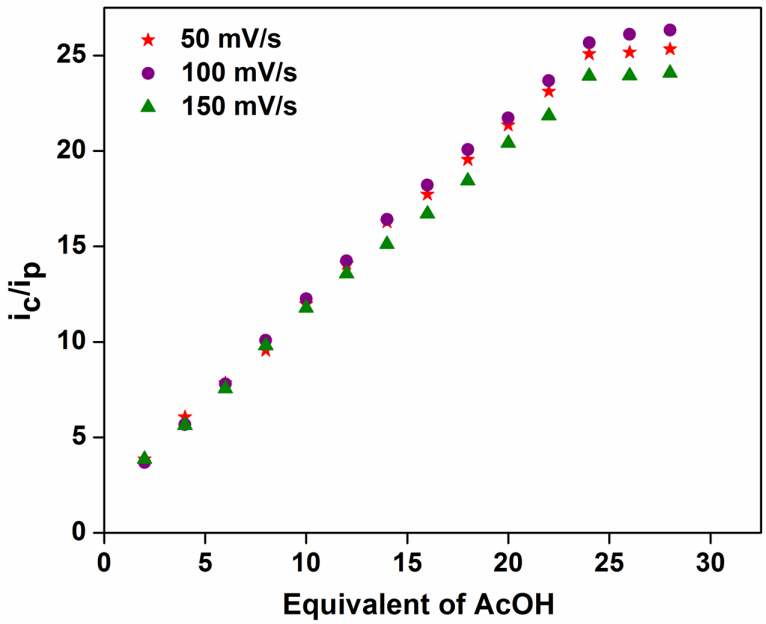

Figure S14. Plot of i_c/i_p *vs.* equivalents of AcOH for three distinct scan rate (50 mV s^{-1}, 100 mV s^{-1} and 150 mV s^{-1}) for **1**. Electrocatalytic condition: 1.0 mM of **1** in 95/5 (v/v) DMF/H_2O in presence of 0.1 M TBAP as supporting electrolyte under inert atmosphere using three-electrode configuration.

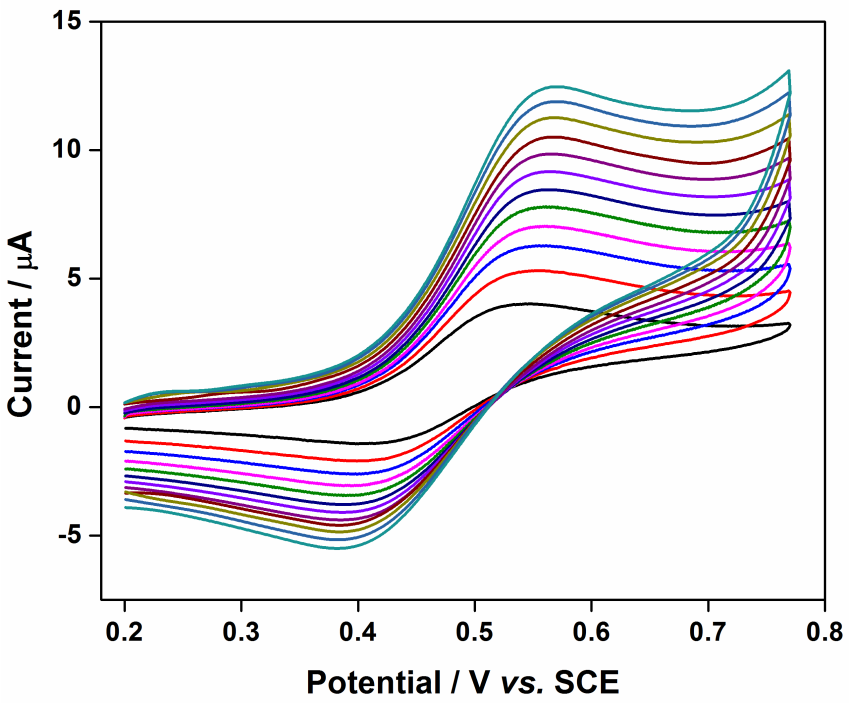

Figure S15. Cyclic voltammograms of 1.0 mM complex **1** in presence of 0.1 M TBAP in 95/5 (v/v) DMF/H_2O at varying scan rates from 25 to 300 mV s^{-1}.

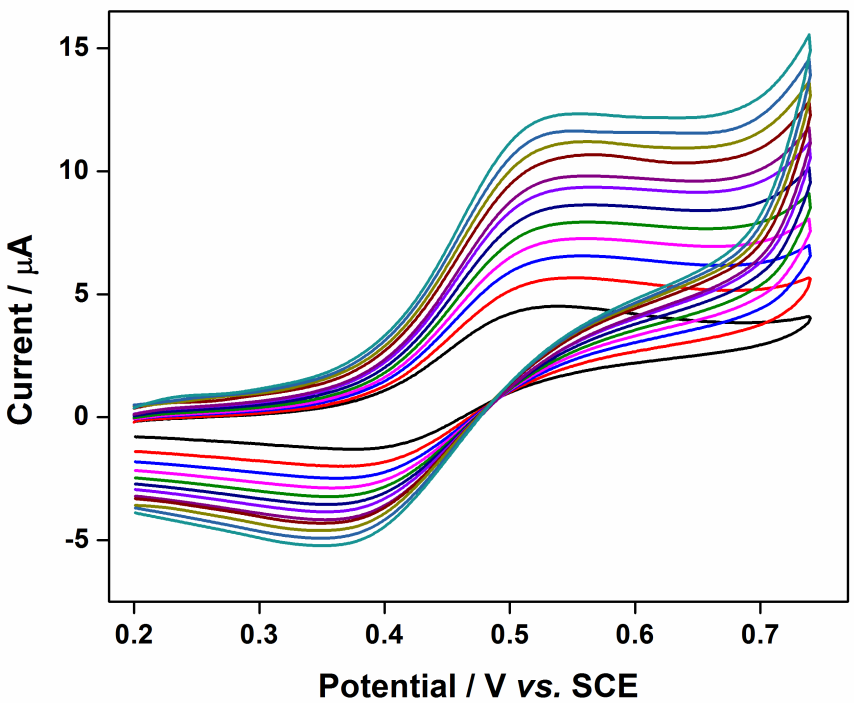

Figure S16. Cyclic voltammograms of 1.0 mM complex **2** in presence of 0.1 M TBAP in 95/5 (v/v) DMF/H_2O at varying scan rates from 25 to 300 mV s^{-1}.

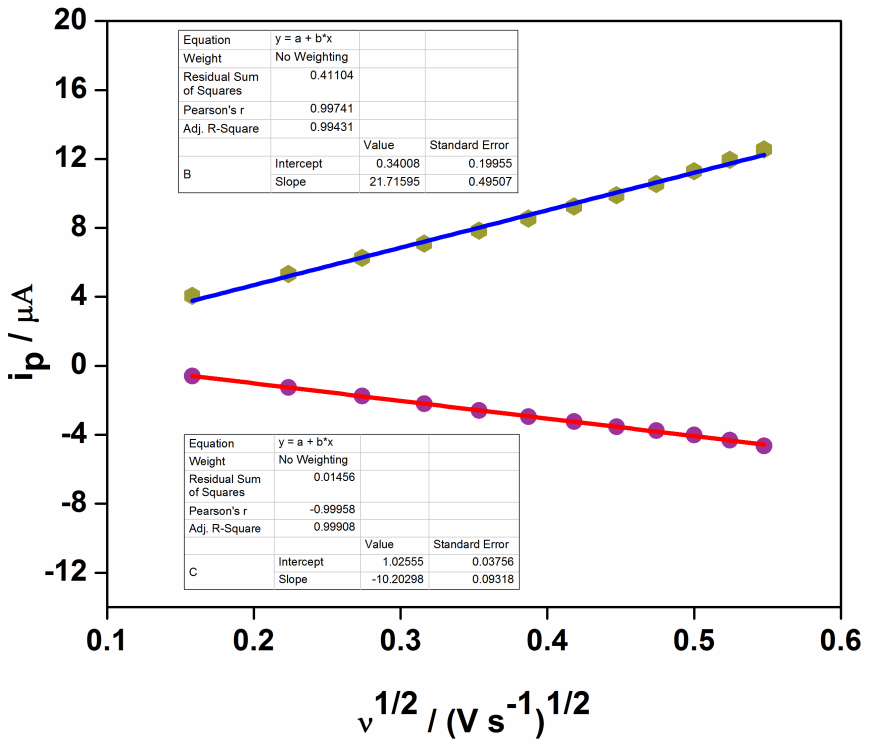

Figure S17. The plot of i_p vs. $\nu^{1/2}$ for **1** with the linear fitted slope for both anodic and cathodic peaks.

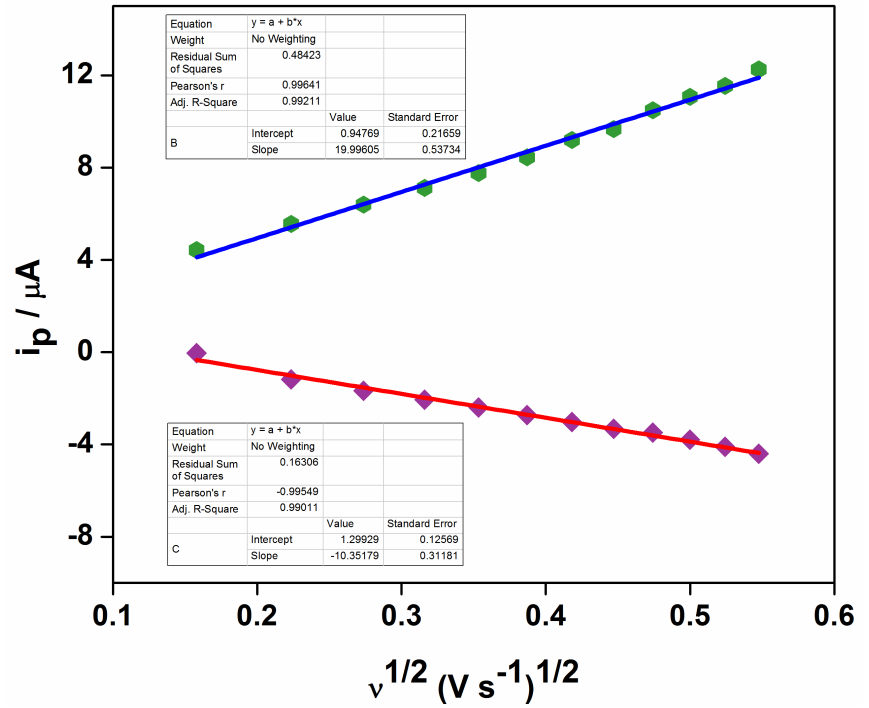

Figure S18. The plot of i_p vs. $\nu^{1/2}$ for **2** with the linear fitted slope for both anodic and cathodic peaks.

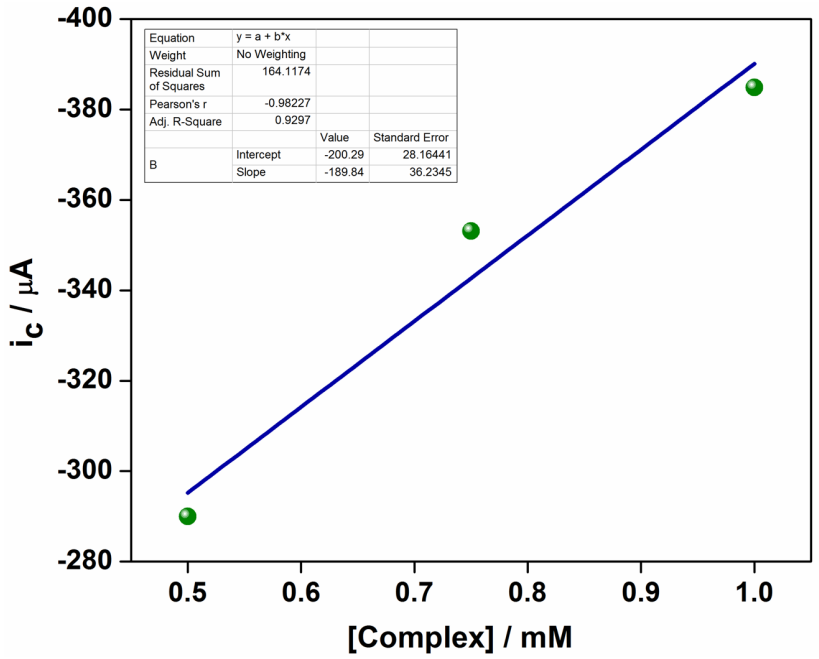

Figure S19. Dependence of catalytic current (i_c) as a function of catalyst concentration of **2** at a fixed AcOH concentration. Electrocatalytic condition: **2** in 95/5 (v/v) DMF/H_2O in presence of 0.1 M TBAP as supporting electrolyte under an inert atmosphere using three-electrode configuration.

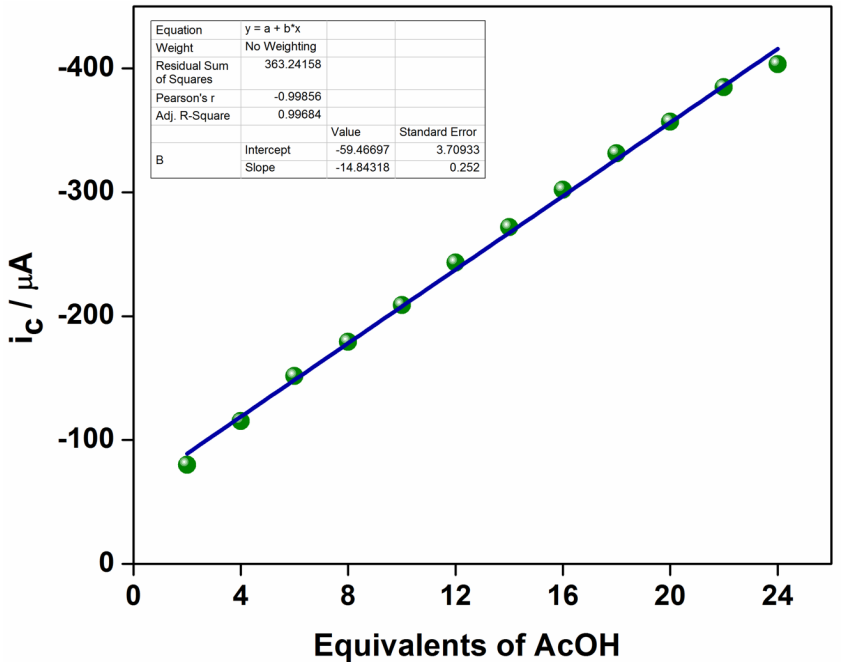

Figure S20. Dependence of catalytic current (i_c) as a function of AcOH concentration for 1.0 mM of **2**. Electrocatalytic condition: **2** in 95/5 (v/v) DMF/H_2O in presence of 0.1 M TBAP as supporting electrolyte under an inert atmosphere using three-electrode configuration.

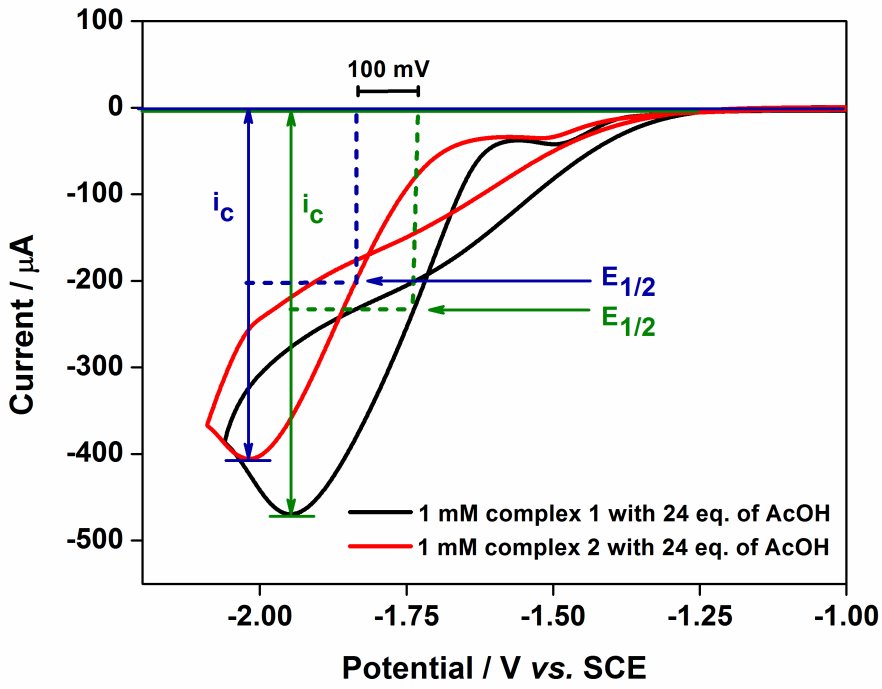

Figure 21. Comparison plot of cyclic voltammogram of complex **1** and **2** in presence of 24 equivalent of AcOH. Electrocatalytic condition: 1.0 mM of complexes in 95/5 (v/v) DMF/H_2O in presence of 0.1 M TBAP as supporting electrolyte at a scan rate of 100 mV s^{-1} under an inert atmosphere using three-electrode configuration.

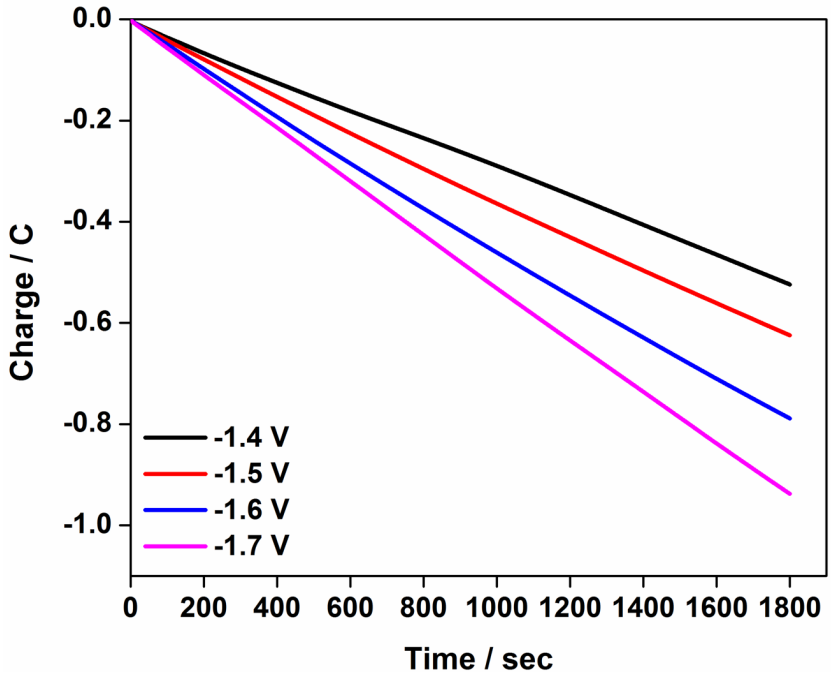

Figure S22. Charge buildup during controlled potential electrolysis of **1**. Electrolysis condition: 0.05mM of **1** with 24 equivalent AcOH in 95/5 (v/v) DMF/H_2O using 0.1 M TBAP as supporting electrolyte under an inert atmosphere for a span of half an hour.

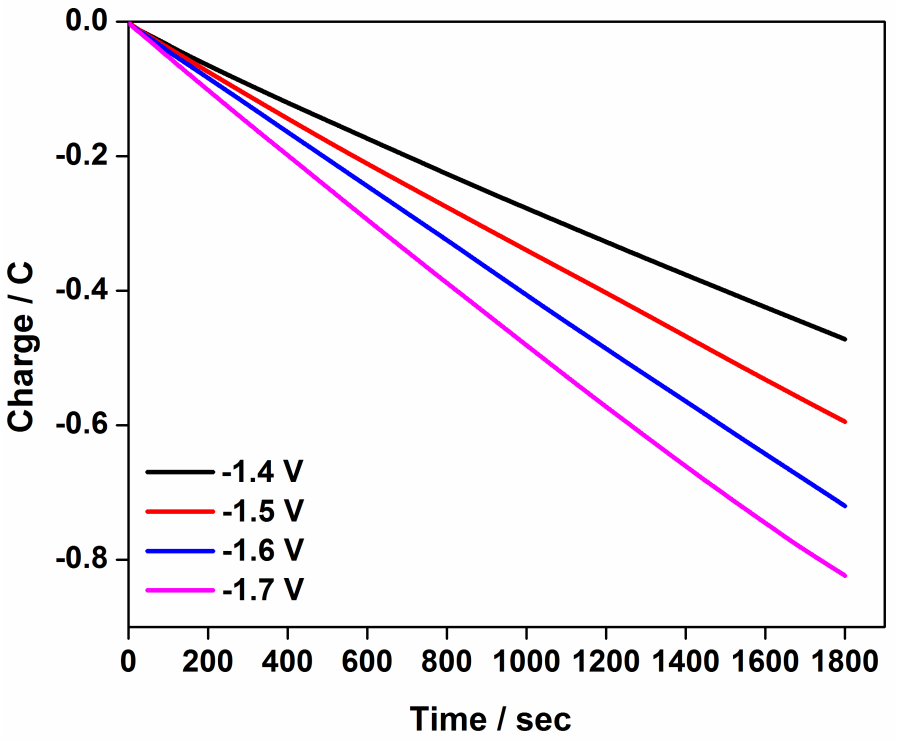

Figure S23. Charge buildup during controlled potential electrolysis of **2**. Electrolysis condition: 0.05mM of **2** with 24 equivalent AcOH in 95/5 (v/v) DMF/H_2O using 0.1 M TBAP as supporting electrolyte under an inert atmosphere for a span of half an hour.

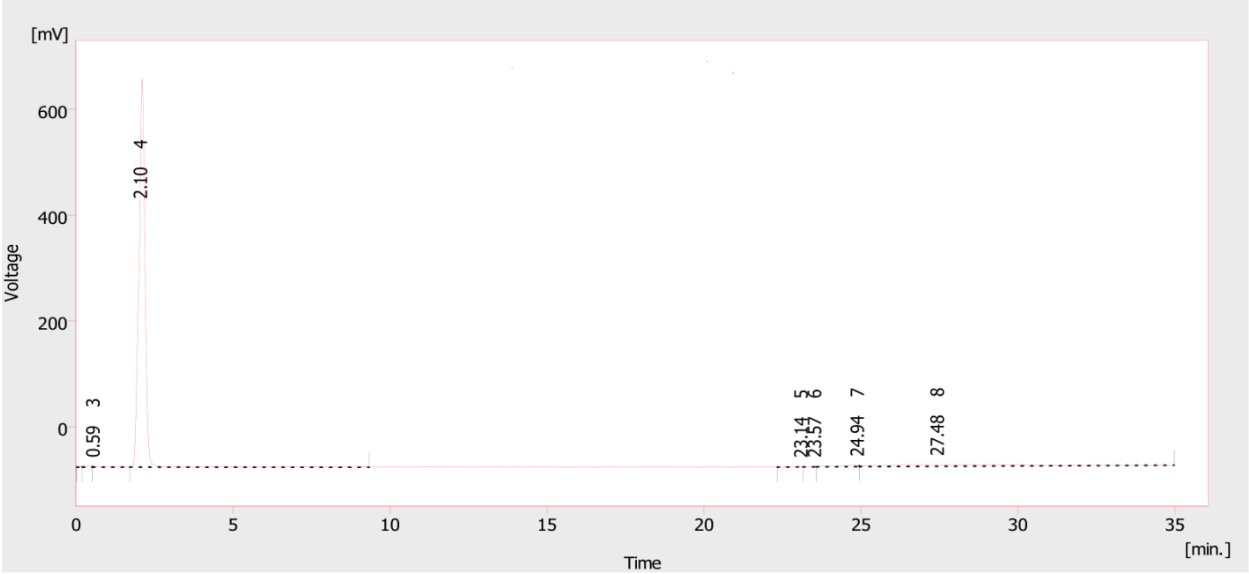

Figure S24. Gas chromatogram of H_2 gas from **1** evolved during the bulk electrolysis process. Electrolysis condition: 0.5mM of **1** with the addition of 24 equivalent AcOH in 95/5 (v/v) DMF/H_2O using 0.1 M TBAP as supporting electrolyte at a potential of -1.7 V vs. SCE under an inert atmosphere for a span of half an hour.

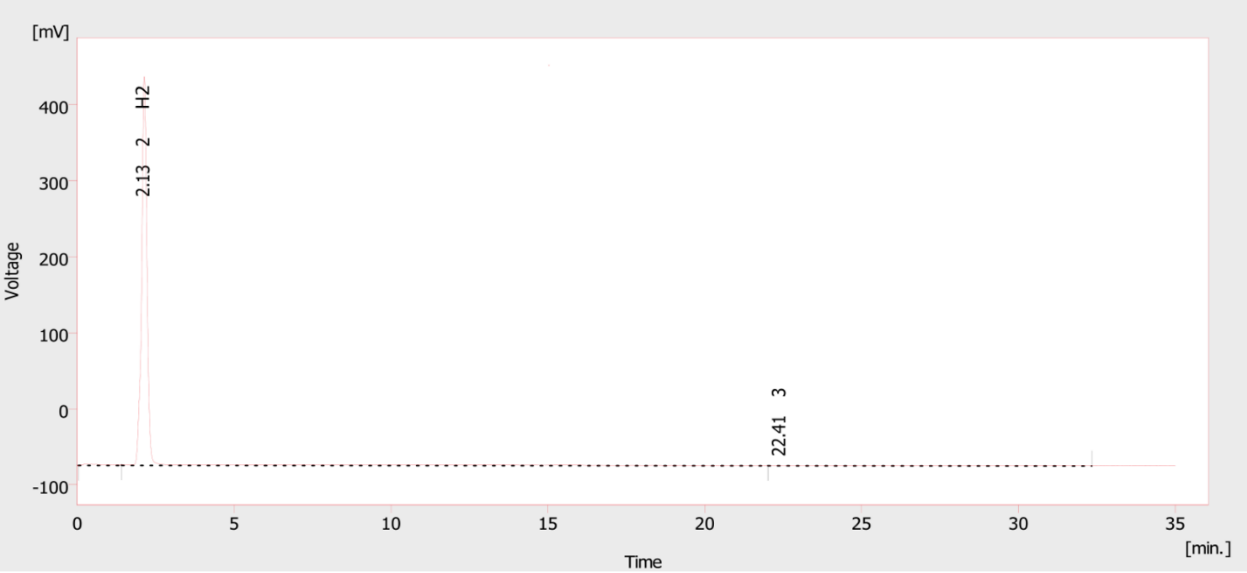

Figure S25. Gas chromatogram of H_2 gas from **2** evolved during the bulk electrolysis process. Electrolysis condition: 0.5mM of **2** with the addition of 24 equivalent AcOH in 95/5 (v/v) DMF/H_2O using 0.1 M TBAP as supporting electrolyte at a potential of -1.7 V vs. SCE under an inert atmosphere for a span of half an hour.

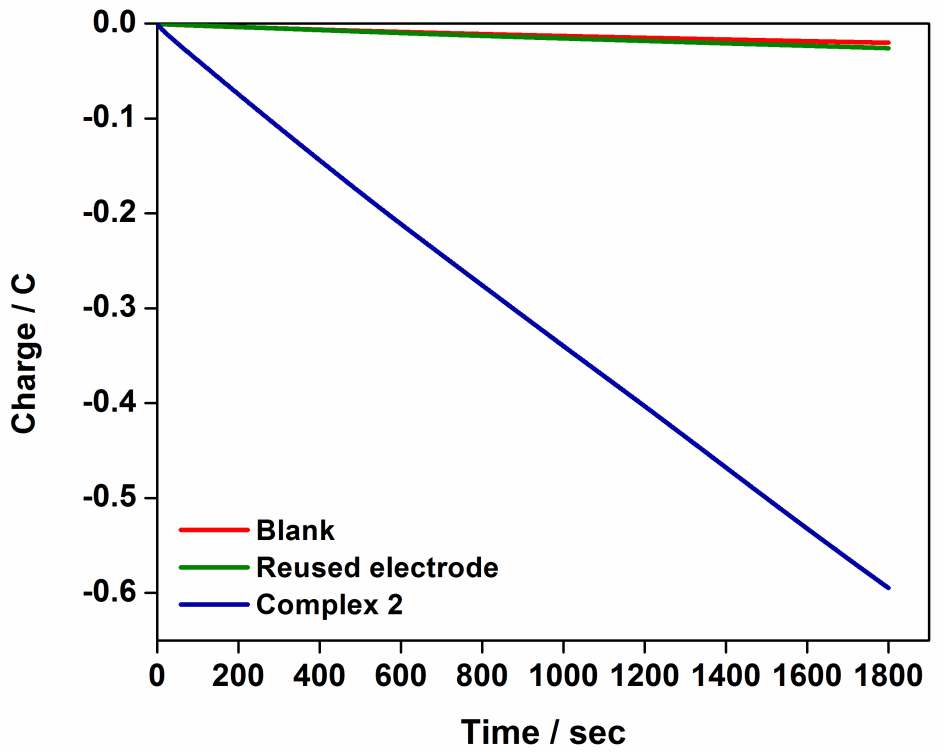

Figure S26. The charge build-up during the controlled potential electrolysis of **2** (blue) and reused electrode after electrolysis (green) at -1.5 V *vs.* SCE. Electrolysis condition: 0.05mM of complex with 24 equivalent AcOH in 95/5 (v/v) DMF/H_2O using 0.1 M TBAP as supporting electrolyte for a span of half an hour.

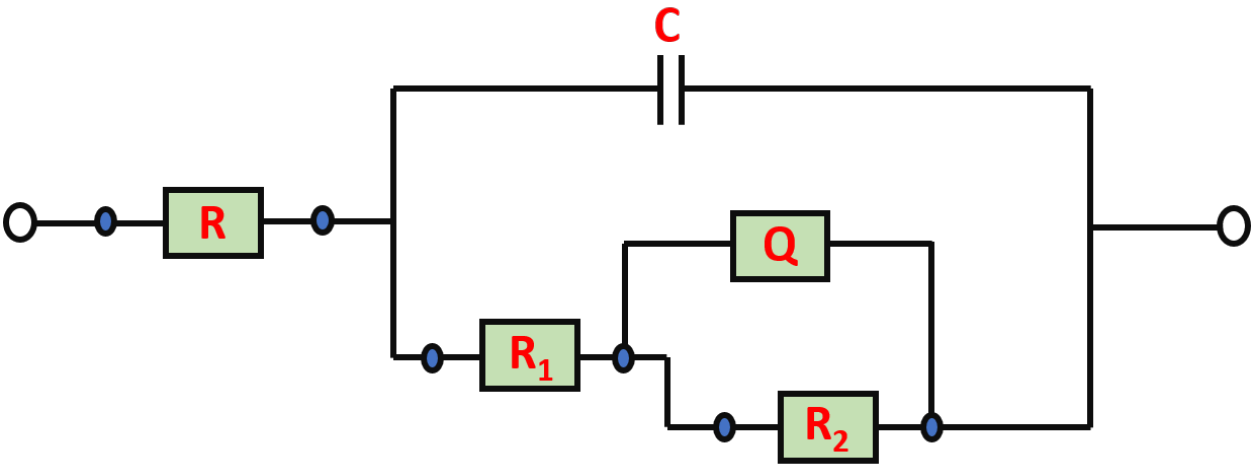

Figure S27. Circuit diagram for the linear fit of Nyquist plot for complex **1** and **2**.

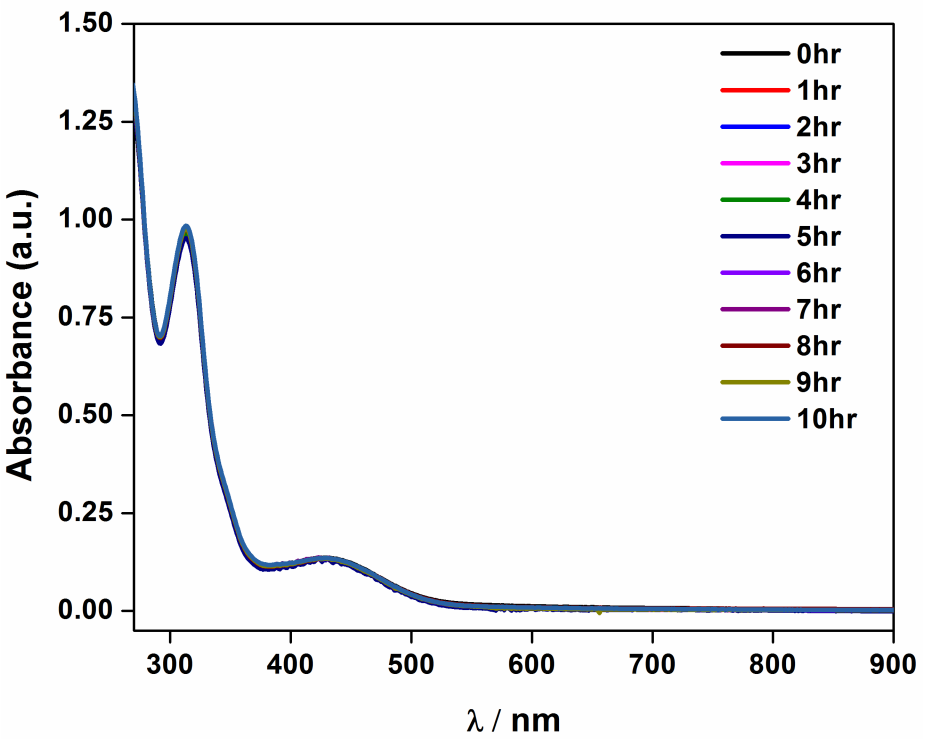

Figure S28. Time-dependent UV-Vis spectra of **1** (0.05mM) in 95/5 (v/v) DMF/H_2O.

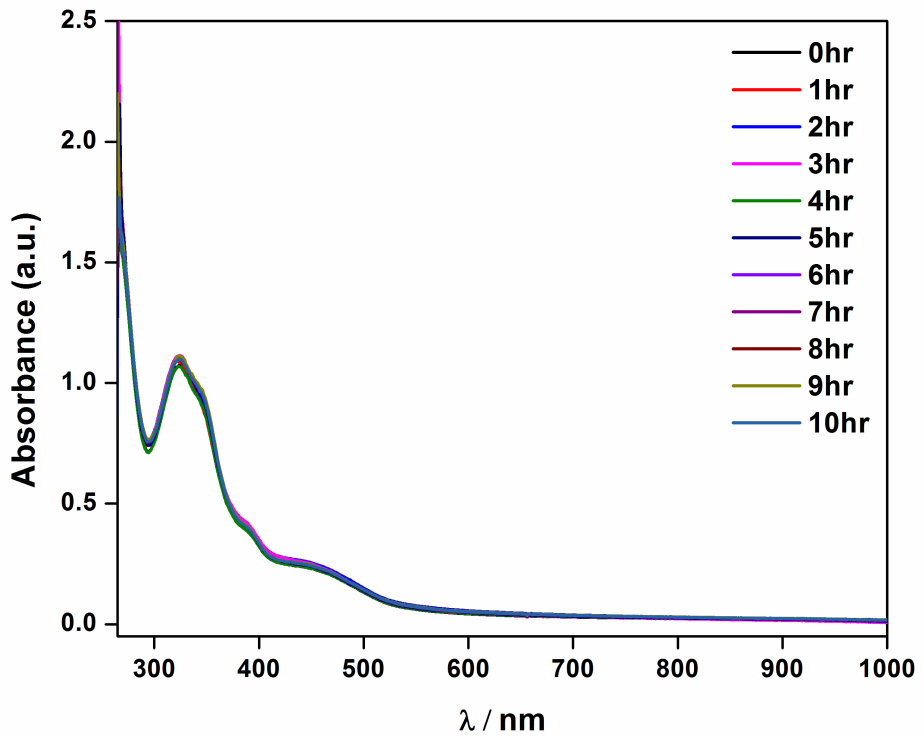

Figure S29. Time-dependent UV-Vis spectra of **2** (0.05mM) in 95/5 (v/v) DMF/H_2O.

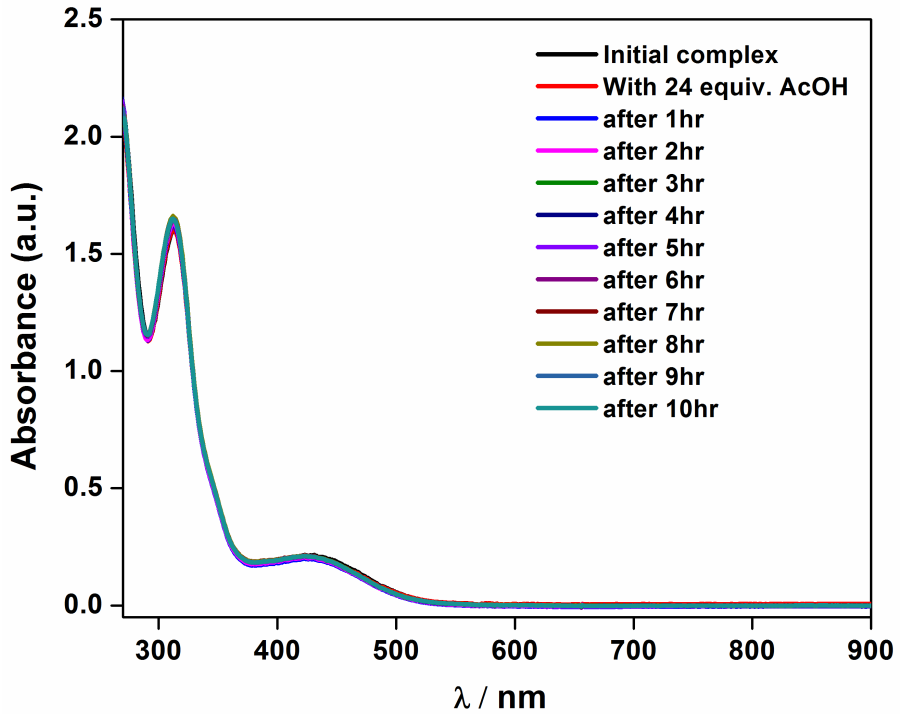

Figure S30. Time-dependent UV-Vis spectra of **1** (0.05mM) in 95/5 (v/v) DMF/H_2O with the addition of 24 equivalent of AcOH.

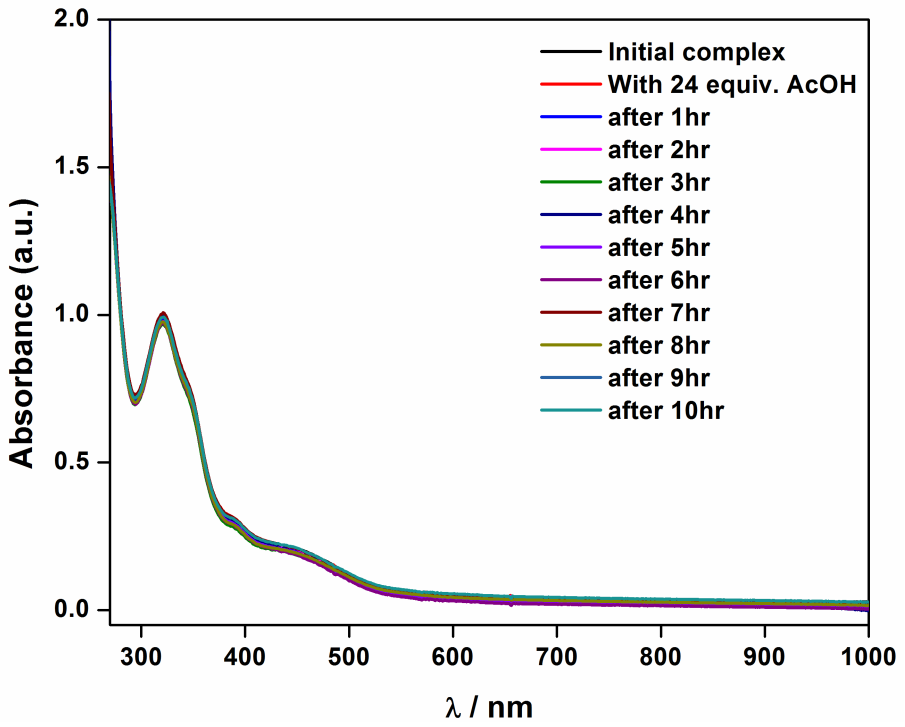

Figure S31. Time-dependent UV-Vis spectra of **2** (0.05mM) in 95/5 (v/v) DMF/H_2O with the addition of 24 equivalent of AcOH.

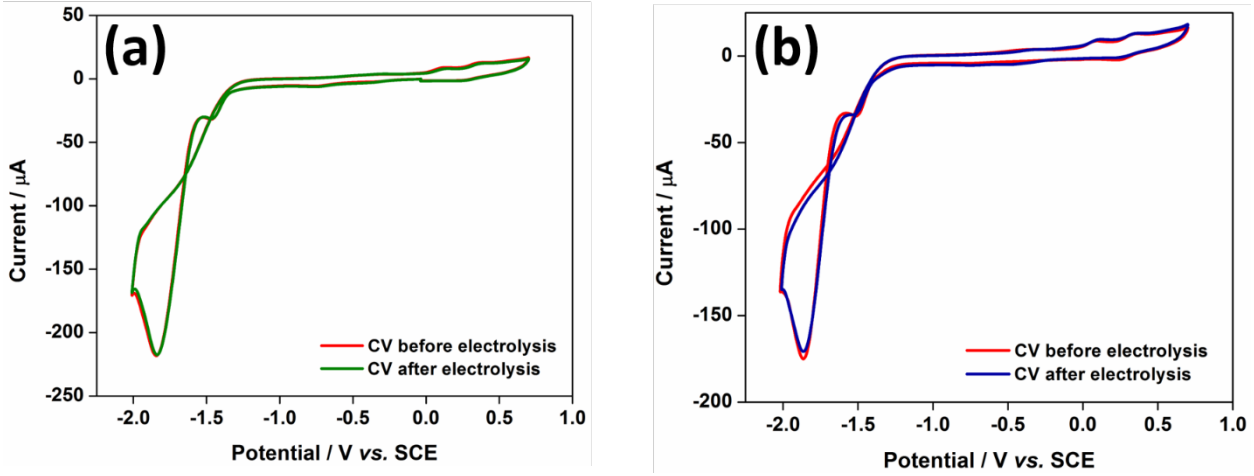

Figure S32. Cyclic voltammogram of complex (a) **1** and (b) **2** before and after the bulk electrolysis for half an hour at -1.5 V *vs.* SCE. Electrolysis condition: 0.05mM of complexes with addition of 24 equivalent AcOH in 95/5 (v/v) DMF/H_2O using 0.1 M TBAP as supporting electrolyte.

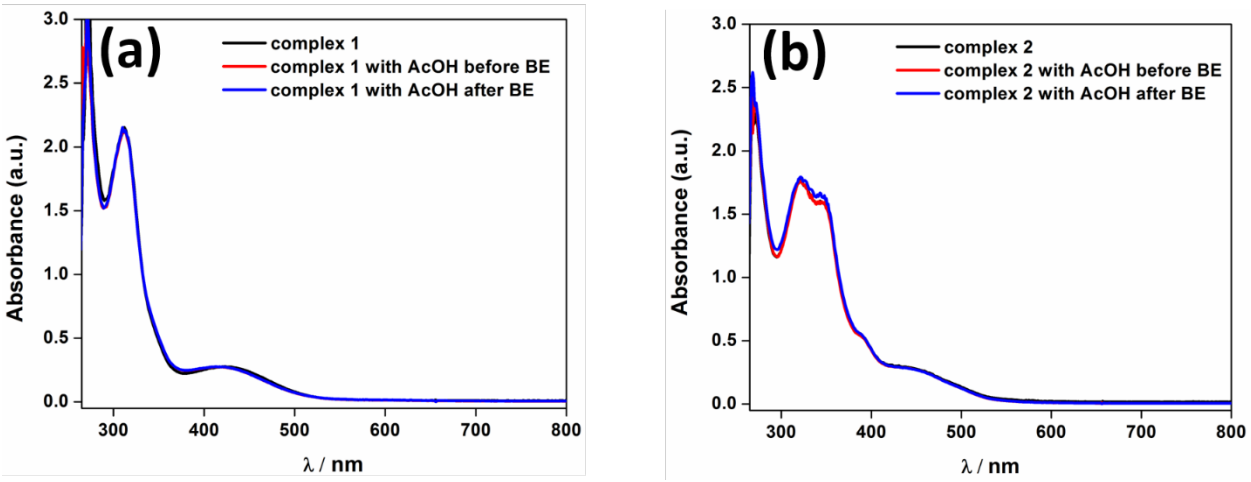

Figure S33. UV-Vis spectra of complex (a) **1** and (b) **2** before and after the bulk electrolysis for half an hour at -1.5 V *vs.* SCE. Electrolysis condition: 0.05mM of complexes with addition of 24 equivalent AcOH in 95/5 (v/v) DMF/H_2O using 0.1 M TBAP as supporting electrolyte.

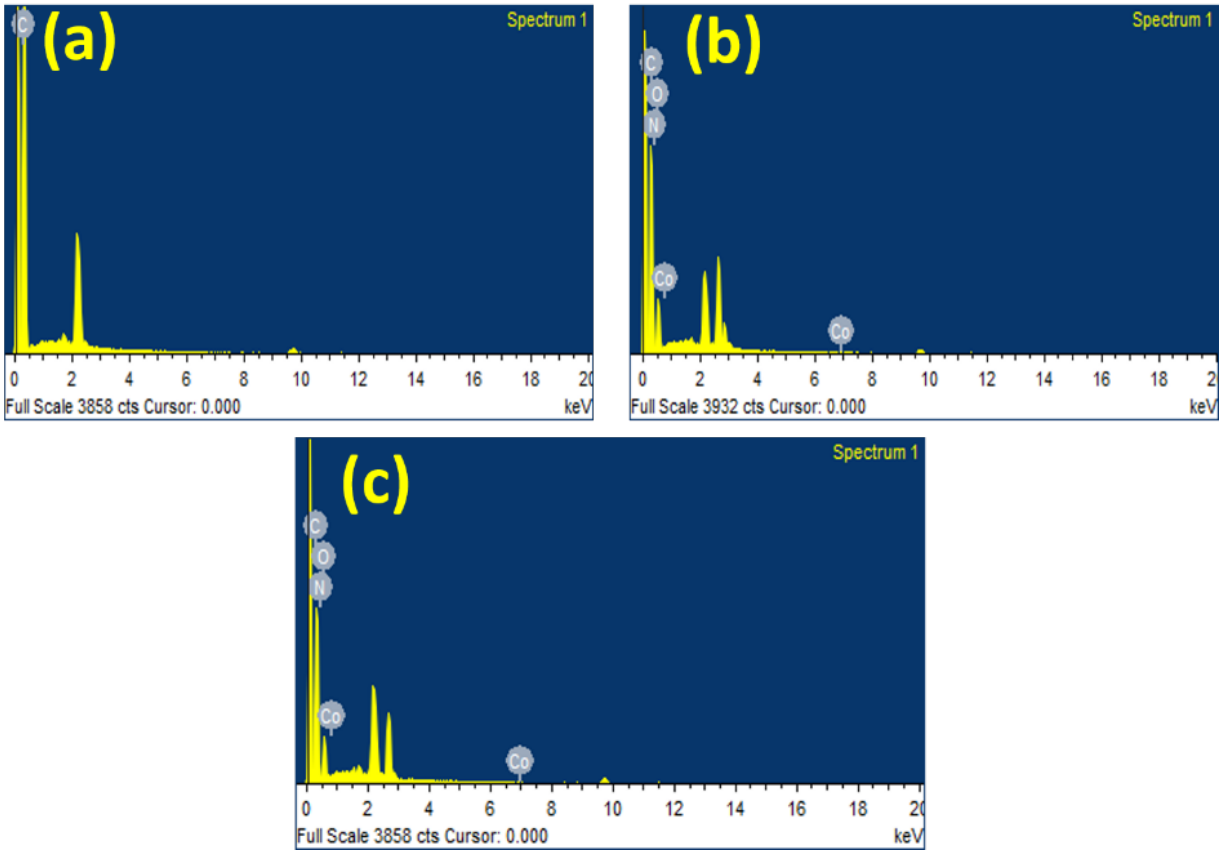

Figure S34. EDX data of glassy carbon plate (a) before bulk electrolysis (b) after bulk electrolysis of **1**, and (c) after bulk electrolysis of **2** for half an hour at -1.5 V vs. SCE. Electrolysis condition: 0.05 mM of complexes with addition of 24 equivalent AcOH in 95/5 (v/v) DMF/H_2O using 0.1 M TBAP as supporting electrolyte. The surface of the electrode was coated with gold to make it current conductive.

Table S7. Atomic and Weight % of elements on the electrode after electrolysis in EDX.

Elements	Blank		Complex 1		Complex 2	
	Weight %	Atomic %	Weight %	Atomic %	Weight %	Atomic %
C	100.00	100.00	51.28	57.79	66.58	72.38
N	--	--	9.76	9.43	6.12	5.70
O	--	--	38.65	32.70	26.70	21.79
Co	--	--	0.32	0.07	0.60	0.13

Calculation

The magnetic susceptibility(X_m) is expressed as follows:

$$X_m = \frac{6}{1000} \times \frac{1}{c} \times \frac{\Delta f}{f}$$

Next, the effective magnetic moment (μ_{eff}) is expressed as follows:

$$\mu_{eff} = 798\sqrt{X_m T} = \sqrt{n(n+2)}$$

where, c = concentration of complex (mol/L)
Δf = shift in the frequency of reference compound (Hz)
f = frequency of spectrometer (Hz)
T = temperature (K)
n = number of unpaired electrons per metal centre

(a) For complex 1:
$c = 2\times10^{-3}$ mol/L
Δf = 0.123 ppm = 49.2 Hz
$f = 400\times10^{6}$ Hz
T = 298 K
Now, $X_{m(\text{complex 1})} = 0.369\times10^{6}$ and $\mu_{eff(\text{complex 1})} = 8.36\ \mu_B$
For, one metal centre $\mu_{eff(\text{complex 1})} = 4.18\ \mu_B$
Thus, $n_{(\text{complex 1})} = 3$.

(b) For complex 2:
$c = 2\times10^{-3}$ mol/L
Δf = 0.109 ppm = 43.6 Hz
$f = 400\times10^{6}$ Hz
T = 298 K
Now, $X_{m(\text{complex 2})} = 0.327\times10^{6}$ and $\mu_{eff(\text{complex 2})} = 7.87\ \mu_B$
For, one metal centre $\mu_{eff(\text{complex 2})} = 3.93\ \mu_B$
Thus, $n_{(\text{complex 2})} = 3$.

References

1. O.V.Dolomanov, L.J. Bourhis, , R.J. Gildea, J.A.K. Howard, & H. Puschmann, (2009), J. Appl. Cryst. 42, 339-341.
2. G.M.Sheldrick, (2015). Acta Cryst. A71, 3-8.
3. G.M. Sheldrick, (2015). Acta Cryst. C71, 3-8.